ENHANCED SAFETY OF AUTONOMOUS DRIVING BY INCORPORATING TERRESTRIAL SIGNALS OF OPPORTUNITY

Mahdi Maaref[†] *Joe Khalife*[‡] *Zaher M. Kassas*[†‡]

[†]Department of Mechanical and Aerospace Engineering, University of California, Irvine, CA, USA
[‡]Department of Electrical Engineering and Computer Science, University of California, Irvine, CA, USA
mmaaref@uci.edu khalifej@uci.edu zkassas@ieee.org

ABSTRACT

A receiver autonomous integrity monitoring (RAIM)-based framework for autonomous ground vehicle (AGV) navigation is developed. This framework aims to incorporate terrestrial signals of opportunity (SOPs) alongside GPS signals to provide tight horizontal protection level (HPL) bounds to enhance the safety of autonomous driving. The performance of the combined GPS-SOP system is analyzed. Simulation results show that the combined GPS-SOP system reduces the HPL significantly from a GPS-only system, particularly in poor user-to-satellite geometry conditions. It is also shown that adding SOPs is more effective in increasing RAIM availability as opposed to adding GNSS satellites. Experimental results show that the GPS-SOP system reduces the HPL by 44.77% from the HPL obtained by GPS-only.

***Index Terms*—** Signals of opportunity, receiver autonomous integrity monitoring, protection level, ground vehicles, navigation, GNSS.

1. INTRODUCTION

Today's autonomous ground vehicles (AGVs) are cocooned in a suite of sensors with different modalities [1, 2]: passive signal-based (e.g., global navigation satellite systems (GNSS)), vision-based (e.g., RGB and IR cameras), dead-reckoning (e.g., inertial navigation system (INS)), and active range-finding (e.g., lidar and radar). These sensing modalities can be classified into two major categories: (i) local sensing modalities, which provide the location of the AGV relative to its own coordinate system and (ii) global sensing modalities, which provide the absolute location of the AGV within a global frame. Navigation systems onboard today's AGVs mainly rely on GNSS, which has monopolized global sensing technologies in outdoor applications for the past few decades. However, in light of recent studies, signals of opportunity (SOPs) have proven to be a particularly fruitful global sensing modality [3–6]. SOPs are radio signals that are not intended for navigation but can be exploited for such purposes [7, 8]. SOPs present a cheap alternative or complement to GNSS, whose signals are challenged in urban environments and could be easily compromised via interference, jamming, or spoofing. Recent results have shown sub-meter-level accurate navigation on unmanned aerial vehicles (UAVs) [9, 10] and meter-level accurate navigation with cellular SOPs for ground vehicles in a standalone fashion [11–13] and in an integrated fashion by aiding an INS [14] or a lidar [15].

This work was supported in part by the Office of Naval Research (ONR) under Grant N00014-19-1-2613 and in part by the National Science Foundation (NSF) under Grant 1929965.

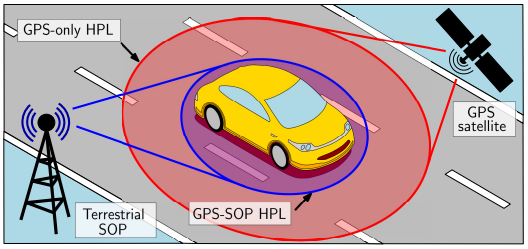

Fig. 1. The proposed framework that combines pseudoranges obtained from GPS satellites and terrestrial SOP transmitters to tighten the HPL.

As vehicles approach autonomous driving with less human-in-the-loop, the trustworthiness of their integrated navigation system becomes ever more critical. According to the SAE J3016 standard, automation levels 4 and 5 require the vehicle to be capable of performing all driving functions independently and self-sufficiently. This level of automation cannot be achieved without a precise measure of trustworthiness of the information given by the sensors onboard the AGV. In the past few decades, the concept of receiver autonomous integrity monitoring (RAIM) was introduced to measure the level of trust in the navigation solution of a GPS receiver. RAIM is a technique based on consistency check of redundant GPS pseudorange measurements, initially investigated in the safety-critical application of aviation. Recently, RAIM for ground vehicles has become the subject of several studies, and many different RAIM schemes incorporating other sensing modalities have been proposed, such as multi-constellation RAIM (e.g., Galileo-GPS [16] and GLONASS-GPS [17]), INS-GPS RAIM [18], lidar-GPS RAIM [19], and INS-lidar RAIM [20]. This article develops RAIM for SOP-GPS to enable safe autonomous driving.

A main objective of RAIM is to alert the user when the protection level (PL), which is a statistical bound on the position error, exceeds a predefined alert limit. The horizontal protection level (HPL) is particularly interesting for AGVs, since it establishes an upper bound on the horizontal position error that holds with a probability greater than some desired integrity risk. A subsequent integrity measure of interest is the availability of a reliable navigation solution, i.e., the fraction of time in which the HPL is less than the horizontal alert limit (HAL). The framework proposed in this article incorporates terrestrial SOPs, whose abundance and favorable geometric configuration help further tighten the HPL and extend the availability period. It is demonstrated numerically and experimentally that fusing terrestrial SOP signals with GPS signals significantly tightens the HPL. Fig. 1 illustrates the proposed GPS-SOP RAIM framework.

An initial work that considered fusing GPS and SOP signals for UAV integrity monitoring was conducted in [21]. This paper ex-

tends [21] through the following contributions. First, in contrast to [21], which considered a single additional transmitter, this work characterizes the RAIM performance after adding multiple transmitters (i.e., a new constellation). This is achieved by incorporating the probability distribution functions of the number of SOPs and the location of SOP towers. Second, in contrast to [21], where the results were presented over a short period of time, this work studies the long-run performance of the proposed GPS-SOP framework using 24-hour period of the recorded GPS data. Third, while [21] only studied the expected reduction in the HPL after incorporating SOP measurements, this work studies both the HPL reduction and the expected increase in RAIM availability. Fourth, this work conducts an experimental test on a ground vehicle showing that even without receiving SOP measurements from negative elevation angles (the case that was studied in [21]) it is still possible to achieve nearly 45% reduction in the HPL.

The paper is organized as follows. Section 2 presents the model description. Section 3 formulates the GPS-SOP RAIM and corresponding HPL parameter. Sections 4 provides simulation and experimental results and analyzes the performance of the proposed framework. Section 5 gives concluding remarks.

2. NAVIGATION FRAMEWORK

This section describes the AGV navigation framework.

2.1. Problem Formulation and AGV State Vector

This paper considers an AGV navigating in an environment comprising N spatially-stationary SOP transmitters with known locations and M GPS satellites. The AGV-mounted receiver makes pseudorange measurements to each of the SOP and GPS transmitters and uses these measurements to (i) estimate its position using a weighted nonlinear least-squares (WNLS) estimator and (ii) calculate the HPL using a RAIM algorithm. It is worth noting that if the AGV is equipped with other navigation sensors, adding SOP pseudoranges via the framework discussed in this paper can still improve the navigation solution and the integrity measures. The AGV-mounded receiver's state vector consists of $\boldsymbol{x}_{\rm AGV} \triangleq \left[\boldsymbol{r}_{\rm AGV}{}^{\mathsf{T}}, c\delta t_{\rm AGV}\right]^{\mathsf{T}}$, where c is the speed of light, $\boldsymbol{r}_{\rm AGV} \triangleq [x_{\rm AGV},\, y_{\rm AGV},\, z_{\rm AGV}]^{\mathsf{T}}$ is the receiver's position expressed in the East, North, Up (ENU) local coordinate frame, and $\delta t_{\rm AGV}$ is the receiver's clock bias.

2.2. GPS Pseudorange Measurement Model

The m-th GPS pseudorange measurement is modeled as

$$\begin{aligned} z_{{\rm GPS}_m}(k) =& \left\|\boldsymbol{r}_{\rm AGV}(k) - \boldsymbol{r}_{{\rm GPS}_m}(k)\right\|_2 + c\cdot\delta t_{\rm iono} + c\cdot\delta t_{\rm tropo} \\ &+ c\cdot\left[\delta t_{\rm AGV}(k) - \delta t_{{\rm GPS}_m}(k)\right] + v_{{\rm GPS}_m}(k), \end{aligned}$$

where $\boldsymbol{r}_{{\rm GPS}_m}$ and $\delta t_{{\rm GPS}_m}$ are the position and clock bias states of the m-th GPS satellite, respectively; $\delta t_{\rm iono}$ and $\delta t_{\rm tropo}$ are the ionospheric and tropospheric delays, respectively; and $v_{{\rm GPS}_m}$ is the GPS measurement noise, which is modeled as a zero-mean white Gaussian random sequence with variance $\sigma^2_{{\rm GPS}_m}$.

2.3. SOP Pseudorange Measurement Model

The n-th SOP pseudorange measurement, after mild approximations discussed in [22], is modeled as

$$\begin{aligned} z_{{\rm SOP}_n}(k) =& \left\|\boldsymbol{r}_{\rm AGV}(k) - \boldsymbol{r}_{{\rm SOP}_n}(k)\right\|_2 \\ &+ c\cdot\left[\delta t_{\rm AGV}(k) - \delta t_{{\rm SOP}_n}(k)\right] + v_{{\rm SOP}_n}(k), \end{aligned}$$

where $\boldsymbol{r}_{{\rm SOP}_n}$ is the position of the n-th SOP transmitter, $\delta t_{{\rm SOP}_n}$ is the clock bias of the n-th SOP transmitter, and $v_{{\rm SOP}_n}$ is the SOP measurement noise, which is modeled as a zero-mean white Gaussian random sequence with variance $\sigma^2_{{\rm SOP}_n}$. Similar to the method discussed in [23, 24], a first-order polynomial approximation is used to model the clock biases $\{\delta t_{{\rm SOP}_n}\}_{n=1}^{N}$, according to

$$\delta t_{{\rm SOP}_n}(k) = \dot{\delta} t_{{\rm SOP}_n}\, kT + \delta t_{{\rm SOP}_{n,0}}, \quad k = 0, 1, \ldots,$$

where T is the sampling period, $\dot{\delta} t_{{\rm SOP}_n}$ is the constant clock drift of the n-th SOP, and $\delta t_{{\rm SOP}_{n,0}}$ is the corresponding initial bias. Modeling of SOP measurements to account for multipath, non-line of sight conditions, and synchronization errors is an active area of research, and has been recently addressed in [24] for cellular SOPs.

2.4. WNLS Estimator Model

A WNLS estimator is used to estimate the AGV-mounted receiver's state vector $\boldsymbol{x}_{\rm AGV}$. The measurement residual computed by the WNLS estimator has a first-order approximation of its Taylor series expansion about $\hat{\boldsymbol{x}}_{\rm AGV}$ given by $\boldsymbol{\Delta z} = \mathbf{H}\,\boldsymbol{\Delta x}_{\rm AGV} + \boldsymbol{v}$, where $\boldsymbol{\Delta z} \triangleq \boldsymbol{z} - \hat{\boldsymbol{z}}$ is the difference between the measurement vector $\boldsymbol{z} \triangleq [z_{{\rm GPS}_1}, \ldots, z_{{\rm GPS}_M}, z_{{\rm SOP}_1}, \ldots, z_{{\rm SOP}_N}]^{\mathsf{T}}$ and its estimate $\hat{\boldsymbol{z}}$, $\boldsymbol{\Delta x}_{\rm AGV} \triangleq \boldsymbol{x}_{\rm AGV} - \hat{\boldsymbol{x}}_{\rm AGV}$, and $\boldsymbol{v} \triangleq [v_{{\rm GPS}_1}, \ldots, v_{{\rm GPS}_M}, v_{{\rm SOP}_1}, \ldots, v_{{\rm SOP}_N}]^{\mathsf{T}}$. The measurement Jacobian used in the WNLS estimator is $\mathbf{H} \triangleq \left[\mathbf{H}^{\mathsf{T}}_{\rm GPS}, \mathbf{H}^{\mathsf{T}}_{\rm SOP}\right]^{\mathsf{T}}$, where

$$\mathbf{H}_{\rm GPS} \triangleq \begin{bmatrix} -\mathsf{c}(el_{{\rm GPS}_1})\mathsf{s}(az_{{\rm GPS}_1}) & -\mathsf{c}(el_{{\rm GPS}_1})\mathsf{c}(az_{{\rm GPS}_1}) & -\mathsf{s}(el_{{\rm GPS}_1}) & 1 \\ \vdots & \vdots & \vdots & \vdots \\ -\mathsf{c}(el_{{\rm GPS}_M})\mathsf{s}(az_{{\rm GPS}_M}) & -\mathsf{c}(el_{{\rm GPS}_M})\mathsf{c}(az_{{\rm GPS}_M}) & -\mathsf{s}(el_{{\rm GPS}_M}) & 1 \end{bmatrix}$$

where $\mathsf{c}(\cdot)$ and $\mathsf{s}(\cdot)$ denote the cosine and sine functions, respectively and $el_{{\rm GPS}_m}$ and $az_{{\rm GPS}_m}$ are the elevation and azimuth angles of the m-th GPS satellites, respectively. The matrix $\mathbf{H}_{\rm SOP}$ has the same form as $\mathbf{H}_{\rm GPS}$, except that $el_{{\rm GPS}_m}$ and $az_{{\rm GPS}_m}$ are now replaced by the elevation and azimuth angles of the n-th SOP transmitter, i.e., $el_{{\rm SOP}_n}$ and $az_{{\rm SOP}_n}$. The weighting matrix in the WNLS is chosen as the inverse of the measurement noise covariance

$$\mathbf{R} = {\rm diag}\left[\sigma^2_{{\rm GPS}_1}, \ldots, \sigma^2_{{\rm GPS}_M}, \sigma^2_{{\rm SOP}_1}, \ldots, \sigma^2_{{\rm SOP}_N}\right],$$

where ${\rm diag}[\cdot]$ denote a diagonal matrix.

3. INCORPORATING SOPS FOR RAIM

This section discusses the GPS-SOP RAIM algorithm for AGV and characterizes its performance.

3.1. RAIM Algorithm

A main objective of RAIM is to detect the presence of a fault, characterized by a bias in the measurement(s), which changes the statistical properties of the residuals. A hypothesis test that considers residual test statistic can be formulated to detect a fault in the system. The resulting test statistic follows a central chi-squared distribution under fault-free operation and a non-central chi-squared distribution under faulty operation. The fault detection can be performed by comparing the test statistic and a threshold [25]. Since the position error is unknown to the RAIM system, it is important to study the sensitivity of the position error to the error in the test statistic. The mapping

between the error in the test statistic domain to the error in the position domain is determined by the so-called "slope", which depends on the satellite-to-receiver geometry and is given by

$$\text{slope}_i = \frac{\sqrt{(\mathbf{B}_{1i})^2 + (\mathbf{B}_{2i})^2} \cdot \sqrt{\mathbf{R}_{ii}}}{\sqrt{\mathbf{S}_{ii}}},$$

where $\mathbf{B} \triangleq \left(\mathbf{H}^\mathsf{T}\mathbf{R}^{-1}\mathbf{H}\right)^{-1}\mathbf{H}^\mathsf{T}\mathbf{R}^{-1}$, $\mathbf{S} \triangleq \mathbf{I} - \mathbf{HB}$, and $\mathbf{X}_{ij}$ denotes the element of i-th row and j-th column of a matrix $\mathbf{X}$. The slope is usually computed for each satellite individually, denoted by slope_i for the i-th GPS satellite. When the slopes are large, the position error becomes more sensitive to the error in the test statistic, making the RAIM system less likely to detect a fault. Therefore, an important quantity to study is the maximum slope, denoted $\text{slope}_{\max}$, to which the HPL is proportional, i.e.,

$$\text{HPL} = \text{slope}_{\max}\sqrt{\lambda_{\text{det}}}, \quad \text{slope}_{\max} = \max\ \{\text{slope}_i\}_{i=1}^{N+M},$$

where λ_{det} is the non-centrality of the test statistic chi-squared distribution under a faulty operation that results in a pre-defined probability of missed detection P_{MD} [21].

3.2. GPS-SOP RAIM Availability

One important integrity measure is the availability a of the RAIM system, which is the probability that satisfies

$$\Pr\left[\text{HPL} \leq \text{HAL}\right] = a,$$

where HAL is set by the application. Ideally, one would like to make the HAL as small as possible while making a as large as possible. Subsequently, the HPL has to be made as small as possible so that a smaller HAL may be set and higher availability may be obtained. One way to reduce the HPL would be by adding more transmitters: either satellites from other GNSS constellations or SOPs. Visible GNSS satellites are usually less abundant than hearable SOPs, and are restricted by an elevation angle mask, denoted by el_{mask}, which is typically around 15°. While adding more measurements from other GNSS satellites decreases the HPL, it will be shown that measurements from terrestrial transmitters at zero elevation angle are more likely to minimize the HPL than transmitters with elevation angles greater than zero. Therefore, adding SOP measurements, which are coming from transmitters at practically zero elevation angle, minimizes the HPL more often than GNSS satellites. This result is validated next through Monte Carlo simulations.

3.3. GPS-SOP RAIM Performance Characterization

It is assumed that the SOPs are long-term evolution (LTE) base stations, i.e., eNodeBs. It has been shown that a binomial point process (BPP) accurately models the distribution of N cellular base stations in an annular region $\mathbb{B}_o\left(d_{\min}, d_{\max}\right)$ where o is the origin, $d_{\min}$ is the far-field distance, and $d_{\max}$ is the maximum distance for which the receiver can reliably hear the SOPs [26] (see Fig. 2(a)). Subsequently, the azimuth angles of the SOPs are uniformly distributed between 0 and 2π (see Fig. 2(b)). For signals in the 800 MHz band and a 1 m antenna array at the eNodeB, $d_{\min} \approx 5$ m. It has been observed experimentally that reliable signals may be tracked at $d_{\max} \approx 3$ km [27]. This model is used to conduct Monte Carlo simulations to characterize the performance of GPS-SOP RAIM.

In each realization, M GPS satellites are randomly placed with azimuth angles generated according to a uniform distribution $az_{\text{GPS}_m} \sim \mathcal{U}(0, 2\pi)$ and elevation angles generated according to

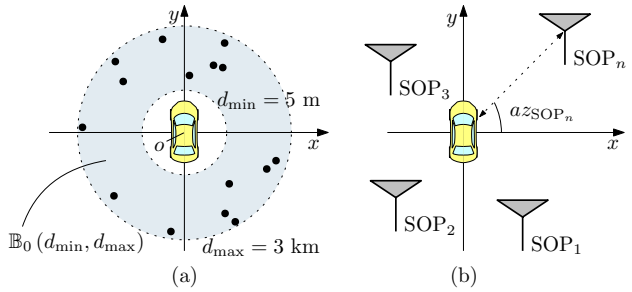

Fig. 2. (a) BPP realization with $N = 15$. (b) The azimuth angles az_{SOP_n} in a BPP are uniformly distributed between 0 and 2π.

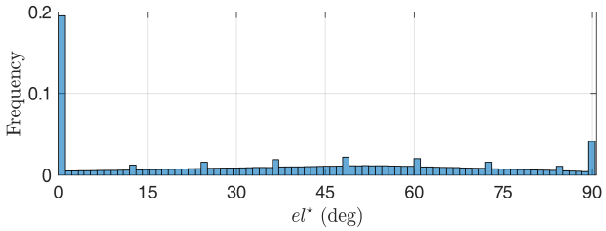

Fig. 3. Monte Carlo simulations showing the histogram of the elevation angle of an additional transmitter that minimizes the HPL for 5 GPS satellites with a 15° elevation angle mask. The histogram was obtained from 10^6 realizations of the azimuth and elevation angles of the 5 GPS satellites and the azimuth of the additional transmitter drawn from uniform distributions.

$el_{\text{GPS}_m} \sim \mathcal{U}\left(el_{\text{mask}}, \frac{\pi}{2}\right)$, for $m = 1, \ldots, M$. Note that these distributions may not accurately model az_{GPS_m} and el_{GPS_m}. However, they will be used in the subsequent analysis for their simplicity and will most likely yield conservative results. Next, one more transmitter is added with a random azimuth angle uniformly distributed between 0 and 2π, and the transmitter elevation angle that minimizes the HPL, denoted by $el^\star$, is obtained by sweeping the range 0 to $\pi/2$. Fig. 3 shows the histogram of $el^\star$ obtained from 10^6 realizations for $M = 5$ and $el_{\text{mask}} = 15^\circ$. It can be seen from Fig. 3 that measurements from terrestrial transmitters (at zero elevation angle) are more likely to minimize the HPL than GNSS satellites.

Next, the HPL cumulative density function (cdf) is characterized for (i) adding N SOP transmitters and (ii) adding N GNSS satellites to M pre-deployed GPS satellites. To this end, M GPS satellites were placed randomly using the distributions discussed earlier. Then, N SOP transmitters were added at 0 elevation angles and random azimuth, and N GNSS satellites were added at random azimuth and elevation angles, distributed according to the aforementioned distributions. Two HPLs were computed: (i) HPL due to SOPs only and (ii) HPL due to GNSS satellites only. The cdfs were computed for both HPLs and are plotted in Fig. 4 for $M = 5$, $el_{\text{mask}} = 15^\circ$, and $N = 4$. Fig. 4 clearly shows the benefit of including SOPs over GNSS satellites, for integrity monitoring. For HAL = 30 m, the availability of RAIM incrases from 81.4% in the case of adding only GNSS satellites to 94.7% for the case of adding only SOPs. It is important to note that HPL is not a measure of the system's accuracy, but of the horizontal position error threshold below which the actual AGV position error remains with probability a. Fig. 4 shows that in order to achieve the same availability as GPS-SOP, the HAL for GNSS only must be set to 46 m, which is more than 1.5 times the HAL for GPS-SOPs. For further HAL tightening, the proposed framework can be coupled with on-board navigation sensors [28].

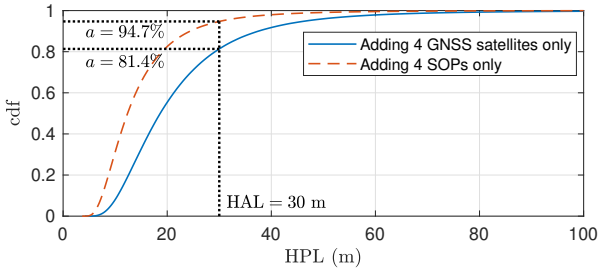

Fig. 4. Monte Carlo simulations showing the cdfs of the HPL when (i) $N = 4$ GNSS satellites are added or (ii) $N = 4$ SOPs are added to $M = 5$ pre-deployed GPS satellites with $el_{\text{mask}} = 15^{\circ}$. The cdfs were obtained from 10^6 realizations. The figure also shows the resulting availability for adding (i) GNSS satellites only and (ii) SOPs only for HAL = 30 m.

4. SIMULATION AND EXPERIMENTAL RESULTS

Simulation results are presented demonstrating the potential of exploiting SOPs for integrity monitoring over a 24-hours. Experimental results are also presented showing the achievable performance of the proposed framework on a ground vehicle.

4.1. Simulation Results

This section presents the simulation results demonstrating the performance of the proposed method. To compare the HPL of a GPS-only solution with that of a GPS-SOP solution, a stationary receiver at the Madrid Deep Space Communications Complex (MDSCC) was considered. The receiver's position was fixed at $\boldsymbol{r}_r \equiv (10^6) \cdot [4.849210, -3.603297, 4.11492]^{\mathsf{T}}$ expressed in an Earth-Centered-Earth-Fixed (ECEF) coordinate frame. The elevation and azimuth angles of the GPS satellite constellation above the receiver over a 24-hour period was computed using GPS ephemeris files collected at the MDSCC. The GPS observations were extracted from the recorded Receiver Independent Exchange Format (RINEX) file. To illustrate the HPL reduction by incorporating SOP observations, 5 SOP transmitters were simulated and the resulting HPL was evaluated. Fig. 5 illustrates the results, which demonstrate that the average GPS-only HPL over 24 hours was 19.45 m, whereas the average GPS-SOP HPL was 11.60 m. Fig. 5 also shows 4 instances where the GPS-only HPL exceeds 40 m due to poor satellite-to-receiver geometry. It can be seen that the HPL is significantly reduced in these instances by incorporating SOP transmitters.

4.2. Experimental Results

An experiment was conducted to demonstrate the proposed navigation framework. To this end, two consumer-grade 800/1900 MHz cellular antennas and a National Instruments (NI) dual-channel universal software radio peripheral (USRP)2954R, driven by a GPS-disciplined oscillator (GPSDO) were used to down-mix and sample LTE signals. The samples were stored on a laptop and then processed by the Multichannel Adaptive TRansceiver Information eXtractor (MATRIX) software-defined reciever (SDR) discussed in [29]. Over the course of the experiment, 5 LTE towers were available. The ground truth was obtained using a Septentrio AsteRx-i V integrated GNSS-IMU system, which was equipped with a dual-antenna, multi-frequency GNSS receiver and a Vectornav VN-100 micro-electromechanical system (MEMS) IMU [30]. Fig. 6 shows the experimental hardware setup and the experiment environment. The WNLS estimator was used to fuse GPS and LTE SOP measurements to estimate the vehicle position and calculate the HPL. The

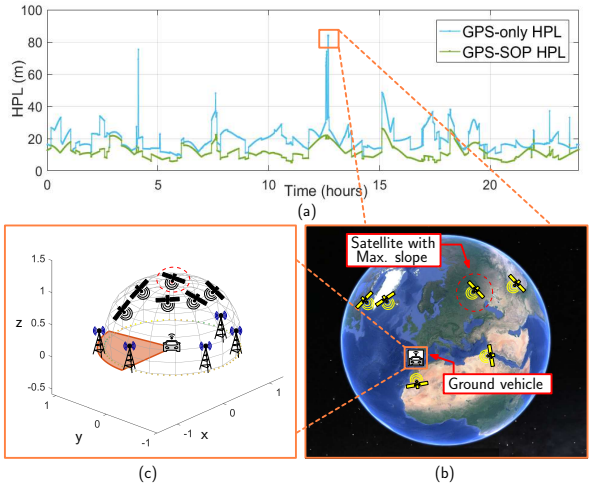

Fig. 5. (a) The HPL obtained from GPS-only versus the proposed GPS-SOP framework over 24 hours. (b) An instance of having HPL $>$ 80 m in the GPS-only framework, which is due to poor satellite-to-receiver geometry. (c) Same instance shown in (b) expressed in ENU coordinate frame centered at the ground vehicle's position.

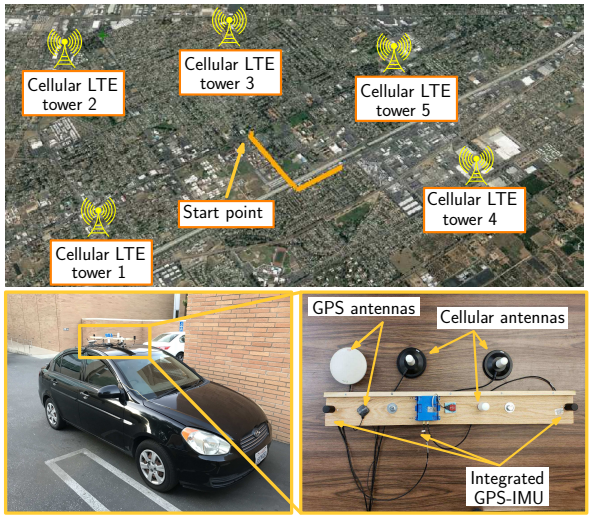

Fig. 6. Experimental hardware setup and the traversed trajectory along with the position of LTE SOP towers.

average GPS-only HPL over the course of the trajectory was 15.01 m, whereas the average GPS-SOP HPL was 8.29 m. Hence, incorporating SOP transmitters reduced the HPL by 44.77%.

5. CONCLUSION

A framework for reducing the AGV's HPL by fusing terrestrial SOPs with GPS was proposed. The framework employed a WNLS to estimate the AGV position and calculate the HPL. Simulation results for a stationary receiver over a 24-hour period were presented showing that the average GPS-only HPL of 19.45 m can be reduced to 11.60 m by incorporating 5 terrestrial SOPs. Experimental results were presented demonstrating that the proposed framework reduced the HPL by 44.77% from the HPL of GPS-only.

6. REFERENCES

[1] T. Luettel, M. Himmelsbach, and H. Wuensche, "Autonomous ground vehicles– concepts and a path to the future," *Proceedings of the IEEE*, vol. 100, no. Special Centennial Issue, pp. 1831–1839, May 2012.

[2] Z. Kassas, P. Closas, and J. Gross, "Navigation systems for autonomous and semi-autonomous vehicles: Current trends and future challenges," *IEEE Aerospace and Electronic Systems Magazine*, vol. 34, no. 5, pp. 82–84, May 2019.

[3] C. Gentner, T. Jost, W. Wang, S. Zhang, A. Dammann, and U. Fiebig, "Multipath assisted positioning with simultaneous localization and mapping," *IEEE Transactions on Wireless Communications*, vol. 15, no. 9, pp. 6104–6117, September 2016.

[4] J. del Peral-Rosado, R. Raulefs, J. Lopez-Salcedo, and G. Seco-Granados, "Survey of cellular mobile radio localization methods: from 1G to 5G," *IEEE Communications Surveys & Tutorials*, vol. 20, no. 2, pp. 1124–1148, 2018.

[5] Z. Kassas, J. Khalife, K. Shamaei, and J. Morales, "I hear, therefore I know where I am: Compensating for GNSS limitations with cellular signals," *IEEE Signal Processing Magazine*, pp. 111–124, September 2017.

[6] Z. Kassas, J. Morales, and J. Khalife, "New-age satellite-based navigation – STAN: simultaneous tracking and navigation with LEO satellite signals," *Inside GNSS Magazine*, vol. 14, no. 4, pp. 56–65, 2019.

[7] J. Raquet and R. Martin, "Non-GNSS radio frequency navigation," in *Proceedings of IEEE International Conference on Acoustics, Speech and Signal Processing*, March 2008, pp. 5308–5311.

[8] Z. Kassas, "Collaborative opportunistic navigation," *IEEE Aerospace and Electronic Systems Magazine*, vol. 28, no. 6, pp. 38–41, 2013.

[9] J. Khalife and Z. Kassas, "Precise UAV navigation with cellular carrier phase measurements," in *Proceedings of IEEE/ION Position, Location, and Navigation Symposium*, April 2018, pp. 978–989.

[10] K. Shamaei and Z. Kassas, "Sub-meter accurate UAV navigation and cycle slip detection with LTE carrier phase," in *Proceedings of ION GNSS Conference*, September 2019, pp. 2469–2479.

[11] C. Yang and T. Nguyen, "Tracking and relative positioning with mixed signals of opportunity," *NAVIGATION, Journal of the Institute of Navigation*, vol. 62, no. 4, pp. 291–311, December 2015.

[12] J. Khalife and Z. Kassas, "Navigation with cellular CDMA signals – part II: Performance analysis and experimental results," *IEEE Transactions on Signal Processing*, vol. 66, no. 8, pp. 2204–2218, April 2018.

[13] K. Shamaei and Z. Kassas, "LTE receiver design and multipath analysis for navigation in urban environments," *NAVIGATION, Journal of the Institute of Navigation*, vol. 65, no. 4, pp. 655–675, December 2018.

[14] Z. Kassas, M. Maaref, J. Morales, J. Khalife, and K. Shamaei, "Robust vehicular navigation and map-matching in urban environments with IMU, GNSS, and cellular signals," *IEEE Intelligent Transportation Systems Magazine*, September 2018, accepted.

[15] M. Maaref, J. Khalife, and Z. Kassas, "Lane-level localization and mapping in GNSS-challenged environments by fusing lidar data and cellular pseudoranges," *IEEE Transactions on Intelligent Vehicles*, vol. 4, no. 1, pp. 73–89, March 2019.

[16] A. Ene, J. Blanch, and T. Walter, "Galileo-GPS RAIM for vertical guidance," in *Proceedings of National Technical Meeting of The Institute of Navigation*, January 2006, pp. 18–20.

[17] T. Walter, J. Blanch, M. Jun Choi, T. Reid, and P. Enge, "Incorporating GLONASS into aviation RAIM receivers," in *Proceedings of International Technical Meeting of the Institute of Navigation*, January 2013, pp. 239–249.

[18] P. Roysdon and J. Farrell, "GPS-INS outlier detection and elimination using a sliding window filter," in *Proceedings of American Control Conference*, May 2017, pp. 1244–1249.

[19] A. Kanhere and G. Gao, "Integrity for GPS-LiDAR fusion utilizing a RAIM framework," in *Proceedings of ION GNSS Conference*, September 2018, pp. 3145–3155.

[20] A. Hassani, N. Morris, M. Spenko, and M. Joerger, "Experimental integrity evaluation of tightly-integrated IMU/LiDAR including return-light intensity data," in *Proceedings of ION GNSS Conference*, September 2019, pp. 2637–2658.

[21] M. Maaref and Z. Kassas, "UAV integrity monitoring measure improvement using terrestrial signals of opportunity," in *Proceedings of ION GNSS Conference*, September 2019, pp. 3045–3056.

[22] Z. Kassas and T. Humphreys, "Observability analysis of collaborative opportunistic navigation with pseudorange measurements," *IEEE Transactions on Intelligent Transportation Systems*, vol. 15, no. 1, pp. 260–273, February 2014.

[23] F. Knutti, M. Sabathy, M. Driusso, H. Mathis, and C. Marshall, "Positioning using LTE signals," in *Proceedings of Navigation Conference in Europe*, April 2015, pp. 1–8.

[24] M. Maaref and Z. Kassas, "Measurement characterization and autonomous outlier detection and exclusion for ground vehicle navigation with cellular signals and IMU," *IEEE Transactions on Intelligent Vehicles*, 2019, accepted.

[25] A. Grosch, O. Crespillo, I. Martini, and C. Gunther, "Snapshot residual and Kalman filter based fault detection and exclusion schemes for robust railway navigation," in *Proceedings of European Navigation Conference*, May 2017, pp. 36–47.

[26] M. Haenggi, J. Andrews, F. Baccelli, O. Dousse, and M. Franceschetti, "Stochastic geometry and random graphs for the analysis and design of wireless networks," *IEEE Journal on Selected Areas in Communications*, vol. 27, no. 7, pp. 1029–1046, September 2009.

[27] J. Khalife, K. Shamaei, S. Bhattacharya, and Z. Kassas, "Centimeter-accurate UAV navigation with cellular signals," in *Proceedings of ION GNSS Conference*, September 2018, pp. 2321–2331.

[28] S. Bhattacharyya and D. Gebre-Egziabher, "Kalman filter-based RAIM for GNSS receivers," *IEEE Transactions on Aerospace and Electronic Systems*, vol. 51, no. 3, pp. 2444–2459, July 2015.

[29] K. Shamaei, J. Khalife, and Z. Kassas, "Exploiting LTE signals for navigation: Theory to implementation," *IEEE Transactions on Wireless Communications*, vol. 17, no. 4, pp. 2173–2189, April 2018.

[30] "Septentrio AsteRx-i V," 2018.